Histidine versus Cysteine-Bearing Heme-Dependent Halogen Peroxidases: Parallels and Differences for Cl – Oxidation

Goedele Roos, Jeremy Harvey

Histidine versus cysteine bearing heme-dependent halogen peroxidases: parallels and differences for Cl^- oxidation

Goedele Roos[a]*, Jeremy N. Harvey[b]

[a],* Dr. Goedele Roos
UGSF - Unité de Glycobiologie Structurale et Fonctionnelle
Univ. Lille, CNRS, UMR 8576
F-59000 Lille, France
E-mail: goedele.roos@univ-lille.fr
0032-3-62531729
[b] Prof. Dr. Jeremy N. Harvey
Department of Chemistry
KU Leuven
Celestijnenlaan 200F
B-3001 Leuven
Jeremy.harvey@kuleuven.be

TOC Graphic

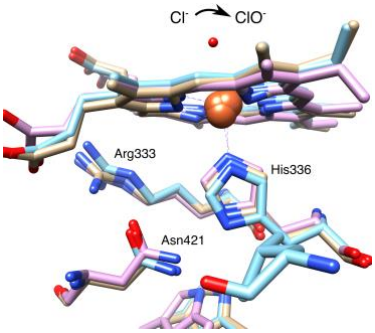

Abstract

The homodimeric myeloperoxidase (MPO) features a histidine as proximal ligand and a sulfonium linkage covalently attaching the heme porphyrin ring to the protein. MPO is able to catalyze Cl^- oxidation with about the same efficiency as chloroperoxidase at pH 7.0. In this study, we seek to explore the parallels and differences between the histidine and cysteine heme-dependent halogen peroxidases. Transition states, reaction barriers and relevant thermodynamic properties are calculated on protein models. Together with electronic structure calculations it gives an overview of the reaction mechanisms, and of the factors that determine the selectivity between one- and two-electron paths. Conclusions point to the innate oxidizing nature of MPO with the ester and sulfonium linkages hiking up the reactivity to enable chloride oxidation. The installation of a deprotonated imidazolate as proximal ligand shifts the does not equilibrium from one- to two-electron events without influencing the chemistry of the oxidation reaction.

Introduction

Heme peroxidases utilize hydrogen peroxide to oxidize organic compounds as an essential step in cell component synthesis and in metabolic and elimination pathways. They also form an essential part of the front-line defense against pathogens of the innate immune system by releasing highly reactive and oxidizing antimicrobial reaction products as hypohalides [1]. In addition, MPO is increasingly reported to play a role in disease pathogenesis, because of its ability to generate reaction products that can oxidize many types of biomolecules such as lipids, DNA and proteins. For an overview of relevant literature, we refer to references given in Soubhye *et al.* [2] and Aldib *et al.* [3].

Peroxidases catalyze one- (Eq. (1)) and two- (Eq. (2)) electron oxidation reactions, corresponding to the so-called “one-electron” and “two-electron” pathways respectively [4].

$$H_2O_2 + 2AH_2 \rightarrow H_2O + 2AH^{\bullet} \qquad (1)$$

$$H_2O_2 + X^- + H^+ \rightarrow H_2O + HOX \qquad (2)$$

In both pathways, the peroxidases undergo a series of redox reactions, hereby cycling in the two-electron pathway through the native enzyme (ferric MPO, Fe (III)) and compound I (oxoiron Fe(IV)=O porphyrin radical cation, Cpd I). In the one-electron pathway, Cpd I is recycled back to the native enzyme through compound II (protonated oxoiron Fe(IV)) (Figure 1). The central redox intermediate Cpd I, is the product of the two-electron oxidation of the native ferric heme by hydrogen peroxide (Eq. (3)).

$$\left[\mathrm{Por}\cdots\mathrm{Fe(III)}\right] + H_2O_2 \rightarrow \left[{}^{\bullet+}\mathrm{Por}\cdots\mathrm{Fe(IV)=O}\right] + H_2O + 2e^- \qquad (3)$$

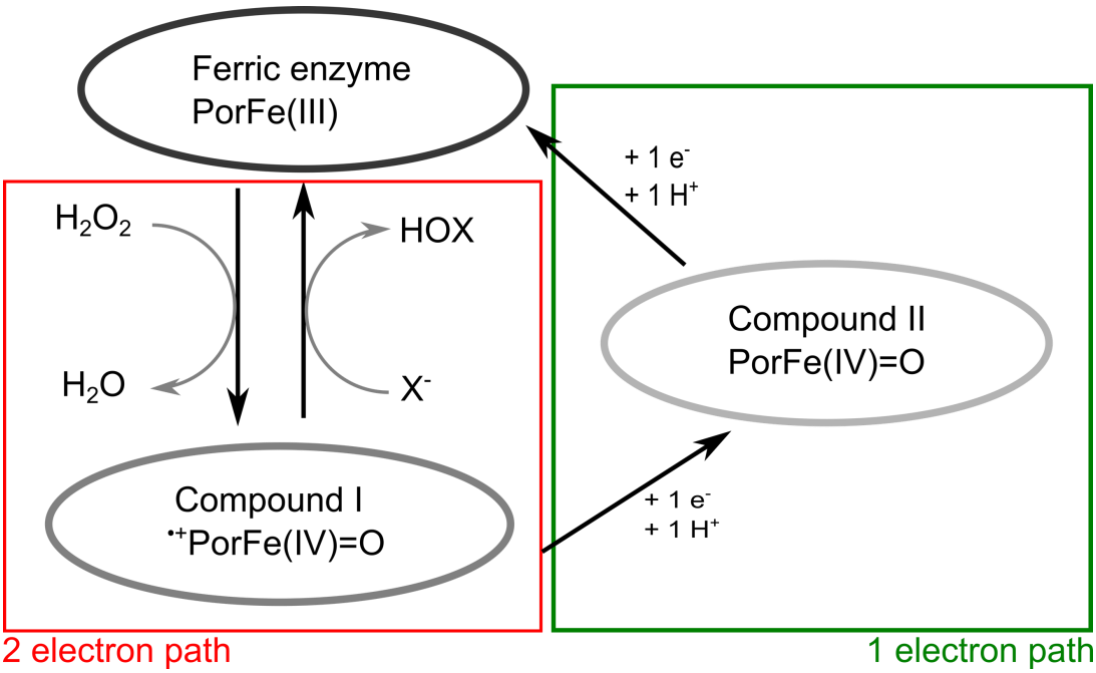

Figure 1 Schematic representation of the one- and two-electron pathways of MPO Reaction 1: ferric MPO (Fe +III; resting state) is oxidized by hydrogen peroxide to compound I (i.e., oxoiron(IV) porphyrin radical cation). Reaction 2: compound I is reduced to compound II (i.e., protonated oxoiron(IV)) by a one-electron donor. Reaction 3: compound II is reduced to the native state, thereby oxidizing a second substrate molecule. Reactions 1, 2, and 3 constitute the peroxidase cycle. Reaction 4: compound I is directly reduced back to the resting state by halides, thereby releasing hypohalous acid. Reactions (1) and (4) constitute the halogenation cycle. Figure adapted from Aldib *et al* [3].

Our focus in this study is to explore the mechanism of two-electron chemistry involved in the oxidation of halides X^- (X= Cl, Br, I) to hypohalides (HOX) catalyzed by Cpd I (Eq. (4)), which is reduced during the reaction to the native enzyme (cfr. Eq. (2)). We also wish to explore which features make a peroxidase well-suited to carrying out this reaction, and determine the competition between the pathways.

$$\left[^{\bullet+}\text{Por}\cdots\text{Fe(IV)=O}\right] + X^- + H^+ \rightarrow \left[\text{Por}\cdots\text{Fe(III)}\right] + \text{HOX} \qquad (4)$$

Two electron chemistry has thus far mainly been reported for heme proteins possessing a negatively charged thiolate or tyrosinate as proximal ligand [5]. The electron donating ligands elevate the pKa of Cpd II and thus lower the one-electron potential of Cpd I [5–7], hereby suppressing one-electron oxidation by shifting the equilibrium from sequential one-electron to two-electron events. This effect, also called the "pushing" effect of cysteine thiolate, by which futile one-electron cycles are avoided, was proposed as underlying mechanism by which C-H bond activation by cytochrome P450 is possible [5,6] and by which catalase can effectively disproportionate H_2O_2 into oxygen and water [7]. For the same reasons, peroxidases with a

(neutral) histidine ligand, having a low Cpd II pKa, typically operate through one-electron reactions [5]. Nevertheless, a number of secreted chordata peroxidases such as myeloperoxidase (MPO), lactoperoxidase (LPO) and eosinophil peroxidase (EPO), which have histidine ligands, are also reported to carry out halogen oxidation. In this study, we seek to explore the parallels and differences between the histidine and cysteine heme-dependent halogen peroxidases.

CPO, a highly versatile heme peroxidase from the marine fungus *Caldariomyces fumago,* has a negatively charged cysteine-derived proximal ligand, similar to the related monooxygenase cytochrome P450 and to nitric oxide synthase (NOS). For an overview of literature on CPO, we refer to references given in Kühnel *et al.* [8]. Halogen peroxidases oxidize X^- to HOX with an apparent second order rate constant of 2.5 10^4 M^{-1} s^{-1} (Table 1), but are also able to catalyze many P450-like oxygen insertion reactions. In general, apparent second order rate constants for reactions of Cpd I with two-electron reductants catalyzed by CPO show attenuated activity compared to P450. For an overview, see Zhang *et al.*[9].

The secreted chordata peroxidases[10] such as the homodimeric myeloperoxidase (MPO), the momomeric lactoperoxidase (LPO) and eosinophil peroxidase (EPO) feature a histidine as proximal ligand and are therefore unique in their ability to efficiently oxidize halides to hypohalides in a two-electron reaction (Table 1) [4]. The proximal histidine in these proteins has been suggested to be deprotonated (and thus negatively charged)[11]. MPO, EPO and LPO are all able to oxidize Br^-, I^- and SCN^-, but only the MPO clade is able to catalyze the production of hypochlorous acid (HOCl) from hydrogen peroxide (H_2O_2) and chloride anions (Cl^-) with about the same efficiency (2.5 10^4 M^{-1} s^{-1}) [4] as reported for CPO at pH 7.0 (Table 1). The $HOCl/Cl^-$ redox couple has an extremely high standard reduction potential $E^{\circ\cdot}$ at pH 7.0 of 1.23 V, while those of other HOX/X^- redox couples are substantially lower: X=Br: 1.13 V; X= I: 0.78 V; X= SCN: 0.56 V. The rate at which Cpd I of MPO is able to oxidize these (pseudo-)halides follows the sequence of their reduction potential.

Table 1: Apparent second order rate constants for Cpd I formation and Cpd I reduction (The MPO, LPO, EPO and HRP data are taken from the more extended Table 4 of the review of Nicolussi *et al.* [10] , we also point to the references given herein). Values are given at pH = 7.0 and 5.0.

Substrate	**MPO**		**MPO E242Q**	**MPO M243V**	**LPO**	**EPO**		**HRP**	**CPO** [9]
Cpd I formation (x 10^4 M^{-1} s^{-1})									
H_2O_2	1800		78	2200	1100	4300		1700	Ca. 400*
Cpd I reduction (x 10^4 M^{-1} s^{-1}) by two-electron donors									
pH	***7.0***[12]	***5.0***[12]	***7.0***	***7.0***	***7.0***[13]	***7.0***[14]	***5.0***[14]	***7.0***	***4.8***
Chloride	2.5	390	0.0065	-	-	0.31	2.60	-	2.5
Bromide	110	3000	5.4	13	41	1900	11000	-	38
Iodide	720	6300	64	1000	1200	9300	> 11000	0.26	n. d.
Thiocyanate	960	7600	22	10000	12000	10000	> 11000	-	n. d.
Cpd I reduction (x 10^4 M^{-1} s^{-1}) by one-electron donors									
Tyrosine (and nitrite)	77		0.0028	n.d.	11	35		5	n. d.

- : No activity measured

n. d.: not determined

*Reported in Araiso *et al.* [15] in Zhang *et al.*[9]

CPO, MPO, LPO and EPO are heme *b* -containing peroxidase having a protoporhyrin IX as basic structure of its prostatic group. MPO's porphyrin ring is covalently attached to the enzyme via two ester bonds (Asp94 and Glu 242) and one electron withdrawing sulfonium linkage (Met 243) (Figure 2)[16]. LPO and EPO only feature the two ester linkages, while the porphyrin in CPO is not linked to the protein. This makes MPO featuring unique post-translational modifications of its heme group.

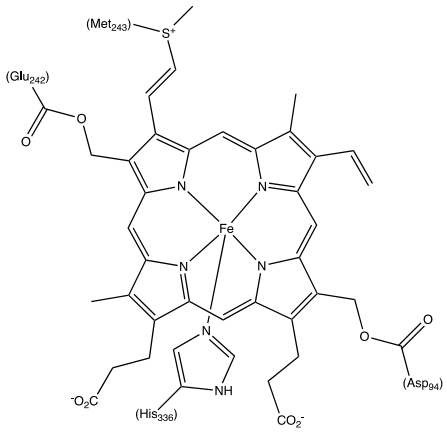

Figure 2 Protoporhyrin IX of MPO in its native ferric Fe(III) state and its covalent attachment to the protein via two ester bonds (Asp94 and Glu242) and one sulfonium linkage (Met243). In addition, the proximal His336 is shown.

Post-translational modifications impose unusual properties of the heme porphyrin. Resonance Raman spectroscopy indicates the enhancement of several out-of-plane low frequency modes by the presence of the ester bonds [17,18]. The UV-Vis absorption spectra of MPO in the Fe(III) in the resting state are characterized by an intense Soret-peak at 428-430 nm [4,10,19–21], which is strongly red-shifted compared to the spectra of other mammalian heme *b* peroxidases having a proximal histidine ligand as LPO[13] and EPO[14] (412-415 nm) and of the horseradish peroxidase (⌴ 403 nm) [10,22], having no post-translational modifications onto its protoporfyrine IX prostatic group (See Table 2 in Nicolussi *et al.* [10] for an extensive overview of electronic absorption maxima of MPO, its mutants and several other peroxidases). This red-shift could be attributed by mutagenesis studies [17,18,21] and by TD-DFT calculations of absorption spectra [23] to the presence of both the esters and sulfonium linkages.

Further, post-translational modifications influence the redox properties of the heme. The presence of the positively charged sulfonium linkage has been linked to the high reduction potentials found for all relevant redox couples of MPO, compared to LPO and other heme b peroxidases (Table 2). For example, typically, the standard reduction potential $E^{\circ'}$ at pH 7.0 of the Fe(III)/Fe(II) redox couple of heme *b* peroxidases is negative (e. g. LPO[24]: -176 mV; HRP[25]: -306 mV) whereas this of MPO is positive (+5 mV) [10,26]. Reduction potential calculations of the FeII/FeIII and Cpd I/Cpd II redox couples show indeed that especially the

sulfonium linkage shifts the potentials to higher positive values[23,27]. The high $E^{\circ'}$ values were suggested to form the thermodynamic basis that enables Cl^- oxidation by MPO [24,26].

Table 2 Standard reduction potentials (pH 7) of all relevant redox couples of MPO, mutant MPO, LPO and horseradish peroxidase (HRP) as example of heme b -containing peroxidases having a histidine as proximal ligand, but not featuring the covalent posttranslational modifications of MPO and LPO. (This table is constructed from Table 3 of the review of Nicolussi *et al.* [10]. We also point to the references given heir in)

$E^{\circ'}$(mV)	Fe(III)/Fe(II)	Cpd I /Fe(III)	Cpd I/Cpd II	Cpd II/Fe(III)
MPO	5	1160	1350	970
CPO[28]	-140 (pH 6.9)	n. d.	n. d.	n. d.
MPO M243V	-182	n. d.	n. d.	n. d.
MPO E242Q	-94	n. d.	n. d.	n. d.
LPO	-176	1090	1140	1040
EPO	-126	1100	n.d.	n.d.
HRP	-306	883	898	869

n. d.: not determined

Based on crystallographic data, it has been argued that the covalent bonds formed between the tetrapyrrole ring and the protein, especially the sulfonium linkage, induce significant distortions of the heme from planarity, [10,11,29] and that this plays a role in determining the reactivity. The first crystal structure of MPO obtained to 1.8 Å resolution has led to the observation that in MPO, the heme group features a pronounced bow-shape structure with low symmetry [10,16,29]. This pronounced out-of-plane distortion has been suggested to cause the different spectral and redox properties of MPO compared to LPO [10].

It is well established that hemes in proteins rarely adopt planar conformations, which are generally conserved within functional classes of proteins[30] and that modulation of ruffling regulates electron transfer with implications for biological activity[31]. For an overview, see Kleingardner *et al.*[32] However, the suggestion that the distortion of the prosthetic group by the sulfonium linkage in MPO gives rise to the highly positive $E^{\circ'}$ values is in contradiction with other studies based on DFT calculations and NMR experiments on ferric Fe(+III) heme. These studies conclude the *decrease* of the heme reduction potential in response to *increased* ruffling[33,34]. Out of plane deformations introduce several changes in the electronic structure of the low-spin His/Met ligated ferric heme cofactor: firstly, the positive spin densities on the β-pyrrole carbon decrease as a function of ruffling. Secondly, the negative spin density on the heme meso carbons decreases in ruffled hemes. Thirdly, all the occupied Fe 3d-based molecular orbitals are destabilized by ruffling, with the Fe-$3d_{xy}$ based MO being the most sensitive. These changes are consistent with the lowering of the Fe(+III)/Fe(+II) reduction potential.

These ambiguities and fragmentary studies present in the current literature towards the oxidation of Cl^- by MPO encouraged us to re-open the investigation to the oxidizing power of MPO.

Computational details

In total, nine models (see Scheme 1, giving an overview) have been constructed to mimic HRP, MPO, LPO and CPO starting from available high-resolution crystal structures with PDB code 5fiw (for the MPO and LPO models) and 2j5m (for the CPO model). For each model, the geometry of all possible spin states of all redox intermediates (resting state, Cpd 0, Cpd I, Cpd II and protonated Cpd II) and of the reactant state (Cpd I.$H_2O.Cl^-$), the transition state (TS) and the product complex (PC) for the oxidation of Cl^- have been fully optimized. IRC calculations show a continuous path from RS, over TS to PC. All geometries were obtained with Gaussian09 [35] at the B3LYP/6-31G(d) level in an SMD solvent model using diethyl ether (ε=4.2400) as solvent. For the MPO^{imi} and HRP^{imi} models, the geometries of the doublet RS, TS and of Cpd II, protonated Cpd II and of the resting state are obtained with Gaussian16 [36]. Several tests confirmed that both versions of the calculation software give similar geometries (atomic distances are the same up to 0.01 Å), varying only a few hundreds to a (few) tenth of one kcal/mol in energy.
Additional single point calculations have been performed at the B3LYP/6-311+(2d,p) level in an SMD solvent model using diethyl ether (ε=4.2400) as solvent, with Gaussian16 [36].
The empirical dispersion correction for density functionals (D3) with Becke and Johnson (BJ) damping has been added during geometry optimization and during single point calculations [37,38].
B3LYP is commonly used and generally accepted as reliable functional [39] for heme systems and found to fairly well reproduce multireference calculations [40,41].
Free energies G^0 were obtained as the sum of the electronic energy (E_{elec}), the zero point energy (ZPE) and a series of thermal correction terms ($G^0 = E_{elec}$ + ZPE+ E_{rot} + E_{vib} + E_{trans} + RT -TS; with S: entropy, R: gas constant, T: temperature and E_{rot} , E_{vib}, E_{trans}: the rotational, vibrational and translational energy), calculated at a standard state of 1 M H^+ and 298.15 K. E_{elec} was calculated at the B3LYP/6-311+(2d,p) D3 BJ level in an SMD solvent model using diethyl ether (ε=4.2400) as solvent. ZPE and thermal correction terms were calculated from partition functions using the harmonic oscillator approximation, in a frequency calculation following the geometry optimization, at the same calculation level. To correct for the breakdown of the rigid rotor harmonic oscillator (RRHO) approximation as approach to calculate the vibrational entropy, all vibrational frequencies below the cut-off value of 50 cm^{-1} were uniformly shifted to 50 cm^{-1} (quasi harmonic approximation as suggested by Cramer and Truhlar et al.[42]).
Reaction free energies $\Delta G^{\circ\prime}$ at pH=7 are obtained from the calculated G^0 values plus $(p'-r')RT\ln 10^{-7}$, making the conversion between the standard state of 1 M H^+ (pH=0) and pH=7. p' and r' are the amounts of H^+ ions respectively formed and used during the reaction.

Results and discussion

To understand the chemistry of Cl^- oxidation by Cpd I for the various heme enzyme models (cfr. eq. (4)), we have studied the transition state, some of the intermediates, and their relevant thermodynamic properties in order to get an overview of the reaction mechanisms, and the factors that determine the selectivity between them. We have chosen a broad range of models (Scheme 1) approximating the heme containing active site of HRP, MPO, LPO and CPO. By choosing a cluster model and the semi-quantitatively accurate B3LYP DFT approach, our study cannot yield quantitative results, but has been designed to provide insights into the chemistry of these peroxidases.

Scheme 1: PPIX models serving as a basis for all the other models: **a.** Minimal model and **b.** the HRP model.

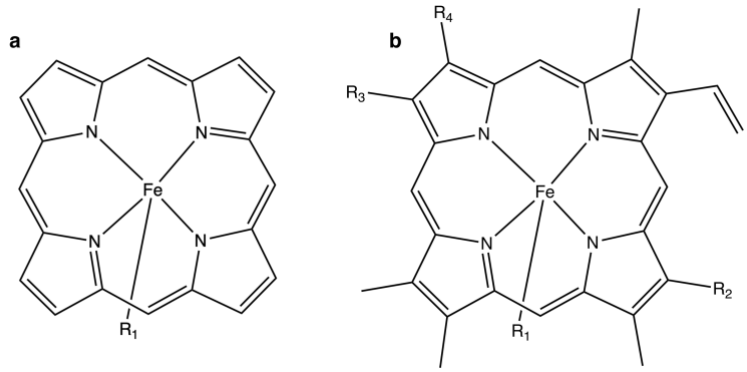

Name of the model				
	R_1	R_2	R_3	R_4
Minimal model	Imidazole	-	-	-
HRP	Imidazole	$-CH_3$	$-CH_3$	$-C_2H_3$
HRP^{imi}	Imidazolate	$-CH_3$	$-CH_3$	$-C_2H_3$
MPO-E242Q	Imidazole	$-CH_3$	$-CH_3$	$-C_2H_2$Met243
LPO	Imidazole	$-CH_2$Asp94	$-CH_2$Glu242	$-C_2H_3$
MPO	Imidazole	$-CH_2$Asp94	$-CH_2$Glu242	$-C_2H_2$Met243
MPO^{imi}	Imidazolate	$-CH_2$Asp94	$-CH_2$Glu242	$-C_2H_2$243
CPO	$-CH_3S^-$ *Cys29*	$-CH_3$	$-CH_3$	$-C_2H_3$
CPO^{envir}	$-CH_3S^-$ *Cys29, Ala31, Leu32* PDB numbering 2j5m	$-CH_3$	$-CH_3$	$-C_2H_3$

In the minimal model, the porphyrin ring of the heme group is used without any side-chains, i.e. with with hydrogen atoms replacing the propionate and vinyl groups and/or their covalently-modified forms present in some of the peroxidases. The proximal histidine ligand is replaced by a (neutral) imidazole group. This core model serves as a basis for all the other models. Its complexity is gradually extended, first by adding the vinyl-groups and -CH_3 groups replacing the propionate groups (HRP model). Secondly, the two ester linkages that are present in LPO and MPO were added (LPO model) and thirdly, the (positively charged) sulfonium linkage is added (MPO model). For CPO, an HRP-like model is constructed, but with the proximal cysteine replaced by (a negatively charged) thiolate.
To investigate the suggested deprotonation of the proximal histidine[11], for both the HRP and MPO models, a second model was built with a negatively charged imidazolate as proximal ligand, the HRP^{imi} and MPO^{imi} models.

Coordinates of the optimized geometries of the redox states participating in the reaction pathways can be found in SI, Table S1. The energetic order of the spin states of Cpd 0, Cpd I and of the resting state has been validated against available literature (Table S2)[39,43]. The lowest energy spin state of each redox intermediate is used to obtain the thermodynamic properties and activation energies, which is the doublet state for Cpd 0 and the quartet/doublet state for the Fe(III) resting state when respectively imidazole or thiolate is present as proximal ligand. Cpd II and its protonated form adopt a triplet ground spin state [44,45]. For the degenerate doublet/quartet state of Cpd I, the quartet state has been chosen (though some additional reactivity calculations were performed for the doublet state).

Reactant state formation

Structure Preceding geometry optimization of the reactant complex (Cpd I.$H_2O.Cl^-$), $H_2O.Cl^-$ was manually positioned at the distal side of the heme. In the optimized geometry, Cl^- accepts a hydrogen bond from the water molecule spanning Cl^- and the oxygen atom of Cpd I. Cl^- is positioned above a meso carbon, at a distance of 2.8 Å to the meso carbon, at 4.8 Å to Fe and at 4.6 Å to the oxygen of Cpd I (distances reported for the optimized MPO model). In structure 1d2v[16], showing bromide binding to the resting state of MPO in a distal cavity 3.5-3.6 Å away from Nε of the distal histidine, Br^- takes a similar position, with a Br^- --- meso carbon distance of 5.6 Å and a Br^- --- Fe (+III) distance of 5.0 Å. All other halides present in structure 1d2v and the halides present in all other available PDB structures are found in cavities remote from the heme[16]. Also for CPO, it has been suggested, based on measured ferric-ferrous redox potentials that are not affected by halide binding[28], that halides do not bind as axial ligand to the ferric heme. As such, halides might first bind into remote binding sites before going to the heme pocket. This questions the assumed reactant complex, especially for CPO, and might lead to erroneous (high) $H_2O.Cl^-$-binding energies calculated in our model system approach (Table 3).

In the given models, a small favorable effect of the ester linkages on Cl^- binding is observed. No direct experimental information on Cl^- binding to Cpd I is available, but the calculated effect of the ester groups agrees with experimental data on cyanide binding to the MPO resting state. The dissociation constants K_D obtained for cyanide binding from respectively kinetic experiments and by spectroscopic titration are 1.9 μM and 1.4 μM for wild type recMPO and 2.4 μM and 3.5 μM for the Glu242Gln mutant, measured at pH=7 and 25°C [46].
$H_2O.Cl^-$ binding seems to be strongly favored in the presence of the sulfonium linkage and strongly disfavored by the presence of the negatively charged thiolate and imidazolate proximal ligands (Table 3). This strong unfavorable binding of Cl^- to CPO is in line with the experimental finding that halides do not bind on axial positions[28]. Some caution is however necessary as the calculated strong effects most probably arise from the approximated models not correctly describing the electrostatic interactions around the ligand's binding.

Electronic structure Cpd I is found to have a 'classic' Cpd I electron configuration, in the models for CPO, MPO and MPO^{imi} that we considered. To show this, we considered orbital coefficients for half-filled orbitals and the Mulliken spin densities (Table 4). The 'classic' electronic structure of Cpd I also extends to the situation where $H_2O.Cl^-$ is bound in the reactant complex. This standard configuration for Cpd I involves the presence of three unpaired electrons, of which two are situated on the Fe-O center, residing in two singly occupied p^*FeO, p^*_{xz} and p^*_{yz}, orbitals, involving anti-bonding interactions between the metal $3d_{xz,yz}$ and the oxygen $2p_{x,y}$ orbitals [39]. The third unpaired electron is located in a high-lying non-bonding porphyrin orbital.
The porphyrin's singly occupied orbital of Cpd I do not mixes with the imidazole/imidazolate orbitals and has merely an A_{1u} character (Figure 3), similar to what was described before for horseradish peroxidase (HRP) [39]. Due to the small mixing of the imidazole/imidazolate orbitals with a_{2u}, the gap between a_{2u} and a_{1u} remains small and thus the gap between the A_{1u} and A_{2u} states remains small. The heme porphyrin in the optimized models with imidazole/imidazolate as proximal ligand is fairly largely distorted from planarity; a distortion that is remarkably more compared to what we observe from our optimized geometries when the charged thiolate is present. These out-of-plane distortions lowers the symmetry of the porphyrin so that the A_{1u} and A_{2u} states can mix their a_{2u} and a_{1u} orbitals and hence also their characters. Upon Cl^- binding to Cpd I, the single occupied porphyrin orbital becomes more localized and is as such a more pronounced a_{2u} orbital. This can also be seen from the localization of the Mulliken spin densities on the meso carbon atoms (Table S3), despite a similar out-of-plane distortion of the porphyrin ring of the Cpd I.$H_2O.Cl^-$ complex compared to Cpd I. The positive spin density present on the substituent vinyl groups of the porphyrin is also removed upon Cl^- binding (Table S3). It is known that many close-lying valence states with different charge distributions, contribute to the electronic structure of Cpd I species[39,47,48]. We assume that the chloride by interacting differently with these valence states perturbs the electronic structure.

For CPO, the singly occupied porphyrin orbital strongly mixes with the donating thiolate ligand in CPO – as was described before for P450 [39]. This mixing is less present when Cl^- is bound. For the CPO model, a drop of the Mulliken spindensity on the CH_3S^- ligand from 0.695 to 0.325 is seen, while the spindensity on the porphyrin ring increases from 0.201 to 0.761 upon $H_2O.Cl^-$ binding.

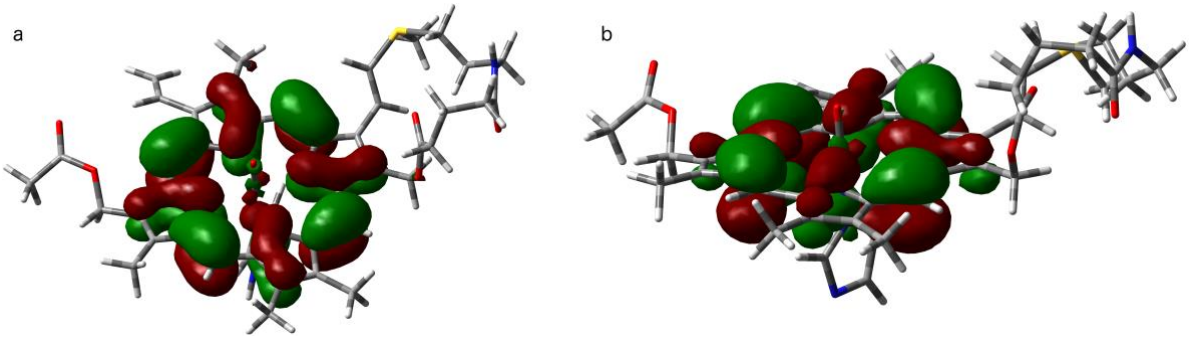

Figure 3: Singly occupied porphyrin orbital (0.02 a. u. isosurface) of Cpd I of the **a**) MPO and **b**) MPO^{imi} model, showing a substantial mixing between the he A_{1u} and A_{2u} states.

Transition state and reaction path

As well as exploring the electronic structure of Cpd 0, I and II, and the thermochemistry of one- and two-electron reaction steps (see next paragraph), we also wish to carry out a preliminary study of the reactivity towards halide (and in particular chloride) oxidation. To do this, transition states (TS) for Cl^- oxidation are obtained for the different heme models and reaction free energies are reported in Table 3. In principle, such oxidation TSs could exist on both the quartet and the doublet potential energy surface. Previous work on analogous two-electron oxidation of sulfide[49] and amines[50] suggests that the doublet TS will lie lower in energy (for oxidation of alkyl halides, however, the quartet TS seems to be lower[51]). In this preliminary study, however, although we have located the doublet TS for one model, we have focused mostly on the quartet TSs, which already provide the required insight into reactivity trends. The doublet TSs proved harder to locate, perhaps because they seem to be low in energy and due to shortcomings in the treatment of the solvation. As previously mentioned, our cluster model and DFT approach precludes reaching quantitative results and seems to affect our ability to study the doublet TS. This also means that our results for reactivity are not quantitative, although trends should be more reliable. For the quartet TSs, a similar structure and electronic structure pattern is found for all of the models (Figure 4). As such, neither the charge of the proximal

ligand nor its nature (imidazole or thiol) nor the heme substituents (covalent ester and sulfonium linkages) seem to influence the nature of the transition state.

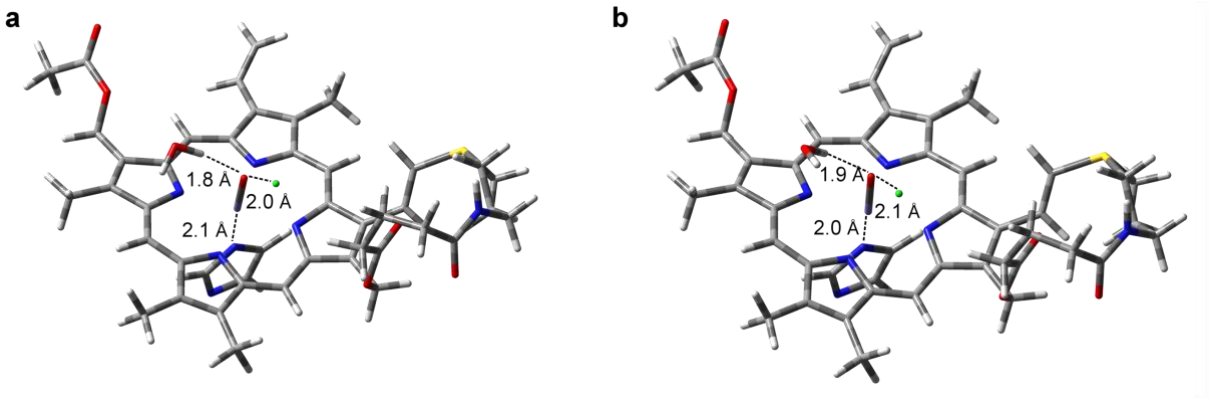

Figure 4: a. Quartet and **b.** doublet transition states of the MPO^{imi} model as representative examples of the TS for Cl^- oxidation catalyzed by MPO. The atoms are colored according to the following code: red: oxygen; grey: carbon; white: hydrogen; blue: nitrogen; yellow: sulfur; green: chlorine

Analysis of the Mulliken spin densities (Table S4) and orbital coefficients point to a product-like TS. The positive spin density on the porphyrin ring and on the oxygen atom, present in the Cpd I reactant state, is removed, while the spin density on Fe increases (compare Table 4 and S4). The doublet MPO^{imi} TS is the lowest energy state, compared to the quartet state. Also, for the product complex, a doublet spin state as ground state is found. As such, the degeneracy between the doublet and quartet spin state found in the reactant state is lifted when evolving to the product complex through the TS. For the oxidation of amines to hydroxylamines [50], the doublet reaction path is also the lowest energy-path, with the degenerate reactant state evolving to a doublet product state through a doublet TS. For the C-H hydroxylation, the doublet and quartet spin state profiles are very close in energy [39].
An IRC (Figure S1a) confirms the continuous path from reactant state to transition state. The analysis of the Mulliken charges (Figure S1b) along the IRC confirms some charge transfer from Cl^- before reaching the TS, although the majority of the charge is transferred after the TS.

Free energy of activation

Table 3 reports the calculated free energies of activation $\Delta G^{\ddagger}$ for the Cl^- oxidation by Cpd I in the given models, which can be related to experimental k_{cat} values. These are not directly available from experiment for the key halide oxidation step, but can be approximately extracted from analysis of the apparent second order rate constants are (Table 1). From these data, we derived the corresponding k_{cat} values (see SI Text S1 for the details of the derivation). It should also be noted that the comparison with experiment is difficult to make in a quantitative way due

to the fact that our models do not provide a definitive treatment of the doublet vs. quartet TSs, and the fact that for some of the models, very strong electrostatic interactions between the chloride and the Cpd I model influence the calculated energies significantly. A rough description of these interactions is included through the use of a microsolvating water molecule for the chloride reactant, and through use of a continuum solvent model. However, based on the large magnitude of the differences in calculated free energies for heme models with different total charge, it is likely that a more accurate treatment would be required in order to obtain even semi-quantitatively accurate free energies. Such a treatment goes beyond the scope of this work, which examines instead the comparative properties of the different peroxidase models.
It is not clear if a reactant state complex is formed and thus both the reactant complex Cpd I.H_2O.Cl^- or the unbound Cpd I + H_2O.Cl^- could be valid choices to take as reference state to calculate the reaction barriers. Reaction barriers relative to both reference states are reported in Table 3 and in the following sections, the barriers with the reactant complex as reference state are discussed. A quantitative discussion of the reactivity would require a more careful investigation of this point.

For CPO, apparent second order rate constants are obtained at pH=4.8 (Table 1). The binding of nitrate, acetate and formate is documented at pH 3 and the dissociation constants are measured to be respectively 0.55 mM, 93 mM and 0.135 mM [52]. Titration results show that halides bind in their anionic form to the acid form of the ferric (Fe +III) enzyme [52]. Based on the size of chloride compared to nitrate/formate versus acetate, we assume a K_M or Cl^- of 0.1 mM. Given the experimentally measured[9] $k_{app} = \frac{k_{cat}}{K_M}$ of 2.5 10^4 M^{-1} s^{-1} , a k_{cat} value of 2.5 s^{-1} can be assumed. This corresponds to an estimated experimental free energy of activation $\Delta G^{\ddagger}$ of 16.9 kcal/mol. For CPO, the existence of a reactant complex is questionable and thus we end up with a calculated activation energy of $\Delta G^{\ddagger,4}$= 44.52 kcal/mol, obviously too high. Optimizing a TS in a model that includes the hydrogen bonding environment around the proximal thiolate was not possible, but the energy values point to a decrease of the reaction barrier when the negative charge is shielded by the environment (Table 3b).

As the binding of chloride to spleen MPO has been found to be pH dependent[53], the experimentally obtained apparent second order rate constant $k_{app'}$ equals :

$$k_{app'} = \frac{k_{cat}}{K_M K_A}\left[H_3O^+\right] \qquad (5)$$

measured at pH = 7.0 and 5.0 for the Cl^- oxidation by MPO (Table 1). Data for K_M are very rare, but an estimate of K_M for Cl^- binding to Cpd I can be made from the available data of Cl^- binding to the resting state of MPO. At room temperature (20° C)[53], K_{Cl^-} is reported to be 0.06 mM; with a p*K*a of the resting state of 3.9. Assuming that binding to the resting state and Cpd

I gives approximately the same values, we can approximate the dissociation constant K_M for chloride as 0.05 mM and K_A as 10^{-4} M. With $[H_3O^+]$ at pH 7 = 10^{-7} M and $k_{app'}$ of 2.5 10^4 $M^{-1}s^{-1}$ (Table 1), k_{cat} equals 0.125 10^4 s^{-1} . For the E242Q mutant, K_M and K_A are assumed to have the same value as for wild type MPO and thus with $k_{app'}$ of 0.0065 10^4 $M^{-1}s^{-1}$ (Table 1), an estimated k_{cat} of 0.0003 10^4 s^{-1} at pH= 7.0 is obtained. These estimated k_{cat} values can now be compared directly to the calculated activation free energies $\Delta G^{\ddagger}$, using the reversed Eyring equation. For MPO, the experimentally estimated $\Delta G^{\ddagger}$ equals 13.2 kcal/mol; for the E242Q mutant, $\Delta G^{\ddagger}$ equals 16.8 kcal/mol, to which the calculated $\Delta G^{\ddagger}$ values (Table 3) largely agrees: for MPO, $\Delta G^{\ddagger,4}$ = 11.76 kcal/mol and for MPO-E242Q $\Delta G^{\ddagger,4}$ = 14.95 kcal/mol. Both values are lower than the $\Delta G^{\ddagger,4}$ of 16.08 kcal/mol calculated for the HRP model, consistent with the experimentally measured oxidation activity (Table 1). The calculated $\Delta G^{\ddagger,4}$ values go together with the electron withdrawing nature of the ester and sulfonium, hereby enhancing the oxidizing power of Cpd I. This is consistent with the increasing/decreasing Mulliken spin density on Cpd I's oxygen/Fe in the presence of the esters and sulfonium (Table 4), allowing the substituted heme to easily accept electrons.

Switching to a charged imidazolate as proximal ligand (HRP^{imi} and MPO^{imi} models), raises the reaction barrier in the quartet path slightly, to 17.73 kcal/mol for the HRP model, and to 14.40 kcal/mol for the MPO model (Table 3). The doublet path for the MPO^{imi} model lowers the barrier to 4.65 kcal/mol. As for CPO, the existence of the assumed reactant state for MPO^{imi} is also questionable. With the unbound Cpd I + $H_2O.Cl^-$ state as reference, the reaction barriers of the doublet and quartet path calculated for the MPO^{imi} model are equal (11 kcal/mol), in agreement with the estimated experimental value of 13.2 kcal/mol.

Thermodynamic properties of reaction intermediates involved in Cl^- oxidation

As depicted in Figure 1, Cpd I can be reduced back to the native ferric state following two competing paths, a one and a two-electron path. A rough estimate of the reactivity of Cpd I in the one-and two-electron cycles comes from the calculation of thermodynamic properties as the one- and two-electron affinity of Cpd I and the proton affinity of Cpd II (Table 5). These calculated properties are approximations for the experimentally measured one- and two- Cpd I reduction potentials (Table 2). As described in the previous paragraph, approximated models are not likely to describe well the electrostatics around the active site and thus, some caution is necessary when discussing the electron affinities. The very negative one-electron affinities of Cpd I in the presence of the sulfonium linkage (MPO E242Q and MPO model) (Table 5) is however consistent with the highly positive $E^{\circ'}$ value of the Cpd I/Cpd II redox couple, experimentally measured to be 1350 mV[54]. The ester groups have only a minor influence on the one-electron affinity, which can't directly be linked to the experimental data of Table 2. The calculated one-electron affinity of Cpd I in the CPO and in the imidazolate bearing models is less negative, indicating a lower one-electron affinity. Also, the presence of the negatively charged chloride ligand, diminishes the one-electron affinity.

These calculated electron affinities follow the sequence of the stability of Cpd I, calculated as the energy difference between Cpd I and Cpd 0 [48].
The two electron reduction potential is much less affected by the sulfonium linkage as is suggested from calculated redox potentials [23] and from the available $E^{\circ'}$ values of the Cpd I/Fe(III) redox couple (Table 2) In agreement with these data, our calculated two-electron affinities of Cpd I in the different models vary less by the presence of the sulfonium linkage than the one-electron affinities (Table 5). The two-electron affinities are calculated to be positive and thus substantially more unfavorable that the one-electron affinities.

One important feature, extensively discussed [5,6,7] as main mechanism to suppress one-electron oxidations by Cpd I, is the pKa of Cpd II. The electron donating proximal thiolate and tyrosinate ligands elevate the pKa of Cpd II as compared to neutral ligands such as histidine. This effect is often referred to as the push-effect. Cpd II's pKa can be estimated by the proton affinity (PA) of Cpd II calculated as the energy difference between its protonated and un-protonated form. The calculated Cpd II PA in models having a neutral histidine as ligand has a substantially less negative value and is thus lower than the Cpd II PA calculated in models having a charged thiolate as ligand. This agrees with experimentally measured Cpd II pKa values of $\pounds$ 3.5 in proteins having a neutral histidine proximal ligand[55,56], while for thiolate and tyrosinated ligated proteins, a high Cpd II pKa of about 12 (P450) - 13 (catalase) has been reported [57,7]. Installing an imidazolate as proximal ligand shifts the Cpd II PA towards more negative values, resembling as such more the Cpd II PA calculated for the CPO models.

Table 3: Reaction free energies $\Delta G^{\circ\prime}$ (kcal/mol) (***a***) and reaction energies (***b***) calculated for the different models with proximal imidazole, imidazolate and thiolate, for the quartet reaction path. G° of the small molecules present in the reaction equations are documented in Table S5.

a

$\Delta G^{\circ\prime}$ (kcal/mol)	Minimal model	HRP	HRP^{imi}	MPO - E242Q	LPO	MPO	MPO^{imi}	MPO^{imi}	CPO
	$=4							***$=2***	***$=4***
Reference state *(2)* *									
Cpd I + $H_2O.Cl^-$	0.00	0.00	0.00	0.00	0.00	0.00	0.00	0.00	0.00
Reaction state ($)									
Cpd I.$H_2O.Cl^-$	9.35	12.05	19.60	1.42	8.99	2.22	11.02	10.77	21.68
TS for Cl^- oxidation ($)									
Cpd I.$H_2O.Cl^-$ (TS)	23.36	28.13	37.33	16.37	24.89	13.98	25.42	15.42	44.52
Product (2)									
Fe(III)+ $H_2O.ClO^-$	2.03	7.41	n.d.	-2.91	13.47	-5.84	n.d.	n. d.	25.33
$\Delta G^{\ddagger,\$}$ (with the reactant state as reference state)	14.01	16.08	17.73	14.95	15.90	11.76	14.40	4.65	22.84

b

ΔE (kcal/mol)	CPO	CPO^{envir}
Reference state *(2)* [*]		
Cpd I + $H_2O.Cl^-$	0.00	0.00
Reaction state (4)		
Cpd I.$H_2O.Cl^-$	10.01	8.43
TS for Cl^- oxidation (4)		
Cpd I.$H_2O.Cl^-$ (TS)	34.63	24.67 [**]
Product (2)		
Fe(III)+ $H_2O.ClO^-$	12.44	n.d.
$\Delta G^{\ddagger,2}$ (with the reactant state as reference state)	24.62	16.24

[*] The used spin state (see main text and Table S2) is given between parenthesis

[**] Estimated from the highest energy scan point obtained in a linear scan of the Cl^- -- O distance starting from the Cpd I reactant state with bound $H_2O.Cl^-$. After identification of the highest energy point, its geometry was subsequently optimized using a frozen optimization procedure to the ground state in which the Cl^- -- O distance was kept frozen to the one of the highest energy point.

n. d.: not determined

Table 4: Mulliken spin density on Fe, oxygen (O) and on the porphyrin ring (Por) of the oxo-iron in the Cl^- bound Cpd I reactant complex (Cpd I.H_2O.Cl^-, quartet spin state).

	Fe	**O**	**Por**
Minimal model	1.280	0.800	0.657
HRP	1.298	0.785	0.698
HRP*imi*	1.300	0.789	0.789
MPO E242Q	1.316	0.783	0.621
LPO	1.298	0.792	0.677
MPO	1.287	0.802	0.676
MPO*imi*	1.293	0.800	0.730
CPO	1.299	0.619	0.761
CPO*envir*	1.278	0.617	0.775

Table 5: Thermodynamic properties (kcal/mol) calculated for the different models with proximal imidazole, imidazolate and thiolate.

ΔE (kcal/mol)	Minimal model	HRP	HRP^{imi}	MPO - E242Q	LPO	MPO	MPO^{imi}	CPO	CPO^{envir}
Properties of Cpd 0 *(2)* *									
Reference state									
Cpd 0 + H^+ + H_2OCl^-	0.00	0.00	n. d.	0.00	0.00	0.00	n. d.	0.00	0.00
Stability of Cpd 0									
Cpd I + H_2O + $H_2O.Cl^-$	-288.66	-295.48	n. d.	-283.03	-292.64	-275.81	n. d.	-317.22	-312.27
Properties of Cpd I *(4)*									
Reference state									
Cpd I + H_2O + $H_2O.Cl^-$	0.00	0.00	0.00	0.00	0.00	0.00	0.00	0.00	0.00
1-electron affinity Cpd I									
Cpd II + H_2O + $H_2O.Cl^-$	-123.67	-116.84	-103.19	-126.92	-119.64	-130.83	-116.99	-92.08	-100.33
Uptake H atom by Cpd I									
Cpd II-OH + H_2O + $H_2O.Cl^-$ - H^+	n. a.	-406.15	-412.85	-405.9	-408.24	-408.30	-414.87	-413.01	-415.65
Properties of Cpd I in presence of Cl^-									
Reference state									
Cpd I.$H_2O.Cl^-$	0.00	0.00	n. d.	0.00	0.00	0.00	n. d.	0.00	0.00
1 electron affinity Cpd I									

Cpd II.$H_2O.Cl^-$ + H_2O	n. a.*	-105.21	n. d.	n. a.*	-108.64	-126.71	n. d.	-72.62	-82.38
Properties Cpd II *(3)*									
Reference state									
Cpd II.$H_2O.Cl^-$ + H_2O	0.00	0.00	0.00	0.00	0.00	0.00	0.00	0.00	0.00
Proton affinity Cpd II									
Cpd II-OH + H_2O + $H_2O.Cl^-$ - H^+	n. a.	-289.32	-309.66	-278.17	-288.60	-277.47	-297.88	-320.93	-315.32

* The used spin state (see main text and Table S2) is given between parenthesis

n. a.: not available, no convergence during geometry optimization of the Cpd II-OH structure

n. a.* : not available, no convergence during geometry optimization of the structure of Cpd II with $H_2O.Cl^-$ bound

n. d.: not determined

Further discussion and perspectives

It seems to be obvious why MPO is a good oxidant. Its porphyrin ring bears electron withdrawing groups in the form of the ester and sulfonium linkages made to the protein. This results – in comparison to other imidazole bearing proteins and to CPO, having a proximal thiolate – in a high/low Mulliken spin density (Table 4) on the oxygen/Fe atoms of its Cpd I, allowing the substituted heme to easily accept electrons, and thus in a low reaction barrier for Cl^- oxidation (Table 3). As depicted in Figure 1, Cpd I can be reduced back to the native ferric state following two competing paths, a one- and a two-electron path. Having a neutral proximal histidine, MPO's Cpd I one-electron affinity is very high (strong negative value, relative to the calculated values for the other models), which is accompanied with a low Cpd II's proton affinity (small negative value, relative to the calculated values for the other models) (Table 5). As such, compared to CPO, MPO's one-electron pathway (Figure 1) seems to be strongly favored over the two-electron oxidation cycle. The question remains how MPO prevents going into these futile one-electron cycles and is as such able to efficiently catalyze the two-electron oxidation of Cl^-. Surprisingly, the answer might lie in the installation of an imidazolate as proximal ligand.

The most obvious choice for the protonation state of the proximal histidine ligand in MPO seems to be the neutral imidazole form. This reasoning is based on earlier work (including QM/MM calculations, Raman spectroscopy and mutagenesis studies) on cytochrome c peroxidase (CcP) [58,59], ascorbate peroxidase (APX)[60,61] and HRP[47], indicating the imidazole rather than the imidazolate nature of the proximal His. The former proteins have a proximal histidine ligand forming a strong hydrogen bond connecting the imidazole's -NH group with the oxygen of an aspartate. In MPO, LPO and EPO, the environment around the proximal His is different. Here, the proximal His is involved in a hydrogen-bond network (Figure 5) with an Asn and Arg, all at Arg-NH_2---OAsn and Asn-NH_2---NHis distances < 3.1 Å, comparable to what has been reported by Carpena, X. *et al* [11].

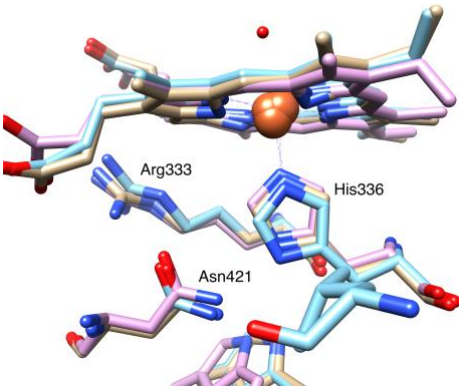

Figure 5: H-bonding environment involving a conserved Asp and Arg around the proximal His in MPO (C atoms in beige), LPO (pink) and EPO (light blue). The MPO (5FIW) and LPO (2Z5Z) are from crystal structures of respectively human MPO and buffalo LPO. The EPO

structure is a homology model constructed for human EPO (Uniprot entry P11678), see SI, text S2 for details.

Structural data and molecular modelling show the -NH_2 group of Asn interacting with N^{δ} of the proximal His, whereas its carbonyl group interacts with Arg at short H-bonding distances. It has been argued that a neutral proximal His would install unfavorable contacts[11,10] at these short distances. In MD simulations with imidazole, the His-Asn-Arg H-bonds are substantially longer. Short His-Asn-Arg hydrogen bond distances are found in all checked crystal structures of MPO and LPO available in the PDB. For EPO, no experimental structures are known, but using homology modelling (for details, see SI text S2), we arrived at a structural arrangement around the proximal His similar to this of MPO and LPO (Figure 5). Also, the ν_{FeHis} stretching mode found in MPO and LPO at fairly high frequencies (248-244 cm^{-1}) might be consistent with a substantial imidazolate character of the proximal ligand in these proteins.

The chemistry of the oxidation reaction is seemingly not influenced by the imidazole/imidazolate character of the proximal ligand: a 'classic' Cpd I electron configuration is found and the (electronic) structures of the TS are similar to these obtained for the other models (Figure 3). Ligation with an electron donating anion - either thiolate, as for example in cytochrome P450 [6] and chloroperoxidases, or tyrosinate as in catalases[7] – has been pointed forward to be crucial for Cpd I to effectively catalyze two-electron oxidations. The electron donating proximal thiolate and tyrosinate ligands elevate the pKa of Cpd II as compared to neutral ligands as histidine. A basic iron(IV)oxo species, installed by anion ligation, minimizes off-pathway chemistry by elevating the pKa of Cpd II, hereby lowering the Cpd I one-electron reduction potential [7]. The relative free energy towards the productive two-electron pathway is as such shifted. Based on Marcus theory, this will suppress the rate constant for one-electron oxidations and thus futile one-electron cycles (Figure 1) are avoided [5,6]. Within the limitations of approximate models, the calculated one-electron affinity of Cpd I and proton affinity of Cpd II (Table 5) seems to point to a similar mechanism for CPO; i. e. disfavoring one-electron chemistry by elevating the proton affinity of Cpd II (as indicator for the Cpd II pKa) and lowering the Cpd I electron affinity (as indicator for the one electron reduction potential of Cpd I). These favorable thermodynamics are also found for the imidazolate bearing models as compared to models with imidazole (Table 5). This can strongly suggest the imidazolate nature of the proximal ligand in MPO, but is on the other hand contradictory to the high one-electron reduction potentials measured for the Cpd I/Fe(III) and the Cpd I/Cpd II redox couples (Table 2). The reaction barriers (when the reactant state complex is taken as reference state) are not influenced strongly by the imidazolate/imidazole nature of the proximal ligand. When the unbound Cpd I + $H_2O.Cl^-$ state is taken as refence state, the reaction barriers with imidazolate are substantially higher than with imidazole as proximal ligand. This reflects most probably the poor description of the Cl^- binding with the electrostatic effect being too large in the imidazolate models. Fully solvated models will be needed to describe correctly the electrostatics. Further, inclusion of specific solvent molecules in the vicinity of the heme will shed light on their possible roles in proton transfer pathways [62].

The calculated $\Delta G^{\ddagger}$ values for all models having an imidazole or imidazolate as proximal ligand are fairly low. Especially the sulfonium linkage has an activating effect, while the ester linkages play only a small activating role. Therefore, LPO and EPO not bearing the sulfonium linkage, but only the ester linkages cannot oxidize Cl^- (LPO) or only to some extent (EPO), but still can oxidize Br^-, CN^- and I^-, having a substantially lower standard reduction potential. HRP, not having the ester linkages does not exert halide oxidation. The calculated $\Delta G^{\ddagger}$ values (Table 3) agrees with this sequence of activity of the oxidation reaction.

Our study, consistent with previous work by Ryde *et al* [23], could not find evidence that out-of-plane distortion of the heme, as has been previously suggested [10,11,29], is at the basis of the ability of MPO to oxidize Cl^-. No convincingly more out-of-plane distortion of the heme porphyrin in the presence of the sulfonium linkage could be observed from visual inspection of the dihedral angles in the porphyrin ring of the optimized geometries of the different model systems.

Obtaining a clear view in the approximated models on the role of Cl^- binding in optimizing the catalytic efficiency ($\frac{k_{cat}}{K_M}$) was also not possible using approximate models. A model for substrate binding to Cpd I has been made based the binding of halides to the cyanide complex of MPO. Energetically similar positions for $H_2O.Cl^-$ at the distal side of the heme pocket can be chosen as starting position, giving raise to structural uncertainties. Also, electrostatic effects might not be fully covered when using approximate models. Electron paramagnetic resonance (EPR) spectra suggest the disruption of the original distal hydrogen bond network in the MPO-CN complex and the involvement of the distal histidine and arginine residues. These data also suggest direct contact between the halide and the iron sixth ligand at low pH only [53,63].
The existence of the Cpd I.$H_2O.Cl^-$ reactant complex might be questionable. This is especially true for CPO for which it has been experimentally suggested that halides do not bind on axial positions[28]. The experimentally obtained K_M data might thus refer to binding in remote pockets and not to heme binding directly. We anticipate this to be a second order effect with an overall impact of going from a remote binding site to the heme pocket on the activation energy presumably being small and based on available experimental data [53,52], we have assumed a K_{Cl^-} in the mili-molar range for both CPO and MPO to estimate the k_{cat}, based on experimentally measured apparent second order rate constants (Table 1) .
To fully judge the effect of out-of-plane distortions and to obtain a clear view on Cl^- binding, studies on entire protein systems should be undertaken.

Conclusion

Although further studies on entire protein systems will be useful to correctly describe the electrostatics and to fully grasp the contribution of ligand binding and heme dynamics on reactivity, we can already conclude from this model-system based study that the histidine bearing MPO has everything to be an as good oxidant as CPO, having a proximal cysteine thiolate. The ester and especially the sulfonium linkages are hiking up the reactivity of MPO to

enable chloride oxidation. The imidazole/imidazolate character of the proximal ligand does not influence the chemistry of the oxidation reaction, but an imidazolate proximal ligand, installed by the H-bonding environment involving a conserved Asp and Arg, instead of a neutral His seems to be necessary to shift the thermodynamic equilibrium from a sequential one-electron to a two-electron event.

Supporting Information

Coordinates of optimized geometries of the redox intermediates: provided as Table S1 in excel-sheet

Word document with: Table S2 – Table S5; Text S1 – S2; Figure S1

Acknowledgement

Computational resources were provided by the Centre de Ressources Informatiques (CRI) of the Université de Lille (France).

References

(1) Klebanoff, S. J. Myeloperoxidase: Friend and Foe. *J Leukoc Biol* **2005**, *77* (5), 598–625. https://doi.org/10.1189/jlb.1204697.

(2) Soubhye, J.; Prevost, M.; Van Antwerpen, P.; Zouaoui Boudjeltia, K.; Rousseau, A.; Furtmuller, P. G.; Obinger, C.; Vanhaeverbeek, M.; Ducobu, J.; Neve, J.; Gelbcke, M.; Dufrasne, F. O. Structure-Based Design, Synthesis, and Pharmacological Evaluation of 3-(Aminoalkyl)-5-Fluoroindoles as Myeloperoxidase Inhibitors. *J Med Chem* **2010**, *53* (24), 8747–8759. https://doi.org/10.1021/jm1009988.

(3) Aldib, I.; Soubhye, J.; Zouaoui Boudjeltia, K.; Vanhaeverbeek, M.; Rousseau, A.; Furtmuller, P. G.; Obinger, C.; Dufrasne, F.; Neve, J.; Van Antwerpen, P.; Prevost, M. Evaluation of New Scaffolds of Myeloperoxidase Inhibitors by Rational Design Combined with High-Throughput Virtual Screening. *J Med Chem* **2012**, *55* (16), 7208–7218. https://doi.org/10.1021/jm3007245.

(4) Furtmuller, P. G.; Zederbauer, M.; Jantschko, W.; Helm, J.; Bogner, M.; Jakopitsch, C.; Obinger, C. Active Site Structure and Catalytic Mechanisms of Human Peroxidases. *Arch Biochem Biophys* **2006**, *445* (2), 199–213. https://doi.org/10.1016/j.abb.2005.09.017.

(5) Yosca, T. H.; Ledray, A. P.; Ngo, J.; Green, M. T. A New Look at the Role of Thiolate Ligation in Cytochrome P450. *JBIC Journal of Biological Inorganic Chemistry* **2017**, *22* (2–3), 209–220. https://doi.org/10.1007/s00775-016-1430-3.

(6) Yosca, T. H.; Rittle, J.; Krest, C. M.; Onderko, E. L.; Silakov, A.; Calixto, J. C.; Behan, R. K.; Green, M. T. Iron(IV)Hydroxide PK(a) and the Role of Thiolate Ligation in C-H Bond Activation by Cytochrome P450. *Science* **2013**, *342* (6160), 825–829. https://doi.org/10.1126/science.1244373.

(7) Yosca, T. H.; Langston, M. C.; Krest, C. M.; Onderko, E. L.; Grove, T. L.; Livada, J.; Green, M. T. Spectroscopic Investigations of Catalase Compound II: Characterization of an Iron(IV) Hydroxide Intermediate in a Non-Thiolate-Ligated Heme Enzyme. *J. Am. Chem. Soc.* **2016**, *138* (49), 16016–16023. https://doi.org/10.1021/jacs.6b09693.
(8) Kühnel, K.; Blankenfeldt, W.; Terner, J.; Schlichting, I. Crystal Structures of Chloroperoxidase with Its Bound Substrates and Complexed with Formate, Acetate, and Nitrate. *Journal of Biological Chemistry* **2006**, *281* (33), 23990–23998. https://doi.org/10.1074/jbc.M603166200.
(9) Zhang, R.; Nagraj, N.; Lansakara-P., D. S. P.; Hager, L. P.; Newcomb, M. Kinetics of Two-Electron Oxidations by the Compound I Derivative of Chloroperoxidase, a Model for Cytochrome P450 Oxidants. *Org. Lett.* **2006**, *8* (13), 2731–2734. https://doi.org/10.1021/ol060762k.
(10) Nicolussi, A.; Auer, M.; Sevcnikar, B.; Paumann-Page, M.; Pfanzagl, V.; Zámocký, M.; Hofbauer, S.; Furtmüller, P. G.; Obinger, C. Posttranslational Modification of Heme in Peroxidases – Impact on Structure and Catalysis. *Archives of Biochemistry and Biophysics* **2018**, *643*, 14–23. https://doi.org/10.1016/j.abb.2018.02.008.
(11) Carpena, X.; Vidossich, P.; Schroettner, K.; Calisto, B. M.; Banerjee, S.; Stampler, J.; Soudi, M.; Furtmuller, P. G.; Rovira, C.; Fita, I.; Obinger, C. Essential Role of Proximal Histidine-Asparagine Interaction in Mammalian Peroxidases. *J Biol Chem* **2009**, *284* (38), 25929–25937. https://doi.org/10.1074/jbc.M109.002154.
(12) Furtmüller, P. G.; Burner, U.; Obinger, C. Reaction of Myeloperoxidase Compound I with Chloride, Bromide, Iodide, and Thiocyanate. *Biochemistry* **1998**, *37* (51), 17923–17930. https://doi.org/10.1021/bi9818772.
(13) Furtmüller, P. G.; Jantschko, W.; Regelsberger, G.; Jakopitsch, C.; Arnhold, J.; Obinger, C. Reaction of Lactoperoxidase Compound I with Halides and Thiocyanate. *Biochemistry* **2002**, *41* (39), 11895–11900. https://doi.org/10.1021/bi026326x.
(14) Furtmüller, P. G.; Burner, U.; Regelsberger, G.; Obinger, C. Spectral and Kinetic Studies on the Formation of Eosinophil Peroxidase Compound I and Its Reaction with Halides and Thiocyanate †. *Biochemistry* **2000**, *39* (50), 15578–15584. https://doi.org/10.1021/bi0020271.
(15) Araiso, T.; Rutter, R.; Palcic, M. M.; Hager, L. P.; Dunford, H. B. *Can. J. Biochem.* **1981**, *59*, 233–236.
(16) Fiedler, T. J.; Davey, C. A.; Fenna, R. E. X-Ray Crystal Structure and Characterization of Halide-Binding Sites of Human Myeloperoxidase at 1.8 A Resolution. *J Biol Chem* **2000**, *275* (16), 11964–11971.
(17) Zederbauer, M.; Furtmüller, P. G.; Brogioni, S.; Jakopitsch, C.; Smulevich, G.; Obinger, C. Heme to Protein Linkages in Mammalian Peroxidases: Impact on Spectroscopic, Redox and Catalytic Properties. *Nat. Prod. Rep.* **2007**, *24* (3), 571–584. https://doi.org/10.1039/B604178G.
(18) Brogioni, S.; Feis, A.; Marzocchi, M. P.; Zederbauer, M.; Furtmüller, P. G.; Obinger, C.; Smulevich, G. Resonance Raman Assignment of Myeloperoxidase and the Selected Mutants Asp94Val and Met243Thr. Effect of the Heme Distortion. *Journal of Raman Spectroscopy* **2006**, *37* (1–3), 263–276. https://doi.org/10.1002/jrs.1442.
(19) Harrison, J. E.; Araiso, T.; Palcic, M. M.; Dunford, H. B. Compound I of Myeloperoxidase. *Biochemical and Biophysical Research Communications* **1980**, *94* (1), 34–40. https://doi.org/10.1016/S0006-291X(80)80183-5.
(20) Kooter, I. M.; Moguilevsky, N.; Bollen, A.; Sijtsema, N. M.; Otto, C.; Wever, R. Site-Directed Mutagenesis of Met243, a Residue of Myeloperoxidase Involved in Binding of the Prosthetic Group. *JBIC Journal of Biological Inorganic Chemistry* **1997**, *2* (2), 191–197. https://doi.org/10.1007/s007750050124.

(21) Kooter, I. M.; Moguilevsky, N.; Bollen, A.; van der Veen, L. A.; Otto, C.; Dekker, H. L.; Wever, R. The Sulfonium Ion Linkage in Myeloperoxidase: DIRECT SPECTROSCOPIC DETECTION BY ISOTOPIC LABELING AND EFFECT OF MUTATION. *Journal of Biological Chemistry* **1999**, *274* (38), 26794–26802. https://doi.org/10.1074/jbc.274.38.26794.
(22) Dunford, H. B.; Dunford, H. B. (Ed). In *Heme Peroxidases*; Wiley-VCH: New York, 1999; Vol. Chapter 4, pp 58–91.
(23) Devarajan, A.; Gaenko, A. V.; Ryde, U. Effect of Covalent Links on the Structure, Spectra, and Redox Properties of Myeloperoxidase – A Density Functional Study. *Journal of Inorganic Biochemistry* **2008**, *102* (8), 1549–1557. https://doi.org/10.1016/j.jinorgbio.2008.01.031.
(24) Furtmuller, P. G.; Arnhold, J.; Jantschko, W.; Zederbauer, M.; Jakopitsch, C.; Obinger, C. Standard Reduction Potentials of All Couples of the Peroxidase Cycle of Lactoperoxidase. *J Inorg Biochem* **2005**, *99* (5), 1220–1229. https://doi.org/10.1016/j.jinorgbio.2005.02.021.
(25) Battistuzzi, G.; Borsari, M.; Ranieri, A.; Sola, M. Redox Thermodynamics of the Fe^{3+}/Fe^{2+} Couple in Horseradish Peroxidase and Its Cyanide Complex. *Journal of the American Chemical Society* **2002**, *124* (1), 26–27. https://doi.org/10.1021/ja017188m.
(26) Arnhold, J.; Furtmuller, P. G.; Regelsberger, G.; Obinger, C. Redox Properties of the Couple Compound I/Native Enzyme of Myeloperoxidase and Eosinophil Peroxidase. *Eur J Biochem* **2001**, *268* (19), 5142–5148.
(27) Battistuzzi, G.; Stampler, J.; Bellei, M.; Vlasits, J.; Soudi, M.; Furtmüller, P. G.; Obinger, C. Influence of the Covalent Heme–Protein Bonds on the Redox Thermodynamics of Human Myeloperoxidase. *Biochemistry* **2011**, *50* (37), 7987–7994. https://doi.org/10.1021/bi2008432.
(28) Makino, R.; Chiang, R.; Hager, L. P. Oxidation-Reduction Potential Measurements on Chloroperoxidase and Its Complexes. *Biochemistry* **1976**, *15* (21), 4748–4754. https://doi.org/10.1021/bi00666a033.
(29) Fenna, R.; Zeng, J.; Davey, C. Structure of the Green Heme in Myeloperoxidase. *Archives of Biochemistry and Biophysics* **1995**, *316* (1), 653–656. https://doi.org/10.1006/abbi.1995.1086.
(30) A. Shelnutt, J.; Song, X.-Z.; Ma, J.-G.; Jia, S.-L.; Jentzen, W.; J. Medforth, C.; J. Medforth, C. Nonplanar Porphyrins and Their Significance in Proteins. *Chemical Society Reviews* **1998**, *27* (1), 31-. https://doi.org/10.1039/a827031z.
(31) Sun, Y.; Benabbas, A.; Zeng, W.; Kleingardner, J. G.; Bren, K. L.; Champion, P. M. Investigations of Heme Distortion, Low-Frequency Vibrational Excitations, and Electron Transfer in Cytochrome c. *Proceedings of the National Academy of Sciences* **2014**, *111* (18), 6570–6575. https://doi.org/10.1073/pnas.1322274111.
(32) Kleingardner, J. G.; Bren, K. L. Biological Significance and Applications of Heme *c* Proteins and Peptides. *Accounts of Chemical Research* **2015**, *48* (7), 1845–1852. https://doi.org/10.1021/acs.accounts.5b00106.
(33) Liptak, M. D.; Wen, X.; Bren, K. L. NMR and DFT Investigation of Heme Ruffling: Functional Implications for Cytochrome *c*. *Journal of the American Chemical Society* **2010**, *132* (28), 9753–9763. https://doi.org/10.1021/ja102098p.
(34) Kleingardner, J. G.; Bowman, S. E. J.; Bren, K. L. The Influence of Heme Ruffling on Spin Densities in Ferricytochromes *c* Probed by Heme Core ^{13}C NMR. *Inorganic Chemistry* **2013**, *52* (22), 12933–12946. https://doi.org/10.1021/ic401250d.
(35) Frisch, M. J. ; T., G. W. ;. Schlegel, H. B. ;. Scuseria, G. E. ;. Robb, M. A. ;. Cheeseman, J. R. ;. Scalmani, G. ;. Barone, V. ;. Mennucci, B. ;. Petersson, G. A. ;. Nakatsuji, H. ;. Caricato, M. ;. Li, X. ;. Hratchian, H. P. ;. Izmaylov, A. F. ;. Bloino, J. ;. Zheng, G. ;.

Sonnenberg, J. L. ;. Hada, M. ;. Ehara, M. ;. Toyota, K. ;. Fukuda, R. ;. Hasegawa, J. ;. Ishida, M. ;. Nakajima, T. ;. Honda, Y. ;. Kitao, O. ;. Nakai, H. ;. Vreven, T. ;. Montgomery, J. A. ,. Jr. ;. Peralta, J. E. ;. Ogliaro, F. ;. Bearpark, M. ;. Heyd, J. J. ;. Brothers, E. ;. Kudin, K. N. ;. Staroverov, V. N. ;. Kobayashi, R. ;. Normand, J. ;. Raghavachari, K. ;. Rendell, A. ;. Burant, J. C. ;. Iyengar, S. S. ;. Tomasi, J. ;. Cossi, M. ;. Rega, N. ;. Millam, N. J. ;. Klene, M. ;. Knox, J. E. ;. Cross, J. B. ;. Bakken, V. ;. Adamo, C. ;. Jaramillo, J. ;. Gomperts, R. ;. Stratmann, R. E. ;. Yazyev, O. ;. Austin, A. J. ;. Cammi, R. ;. Pomelli, C. ;. Ochterski, J. W. ;. Martin, R. L. ;. Morokuma, K. ;. Zakrzewski, V. G. ;. Voth, G. A. ;. Salvador, P. ;. Dannenberg, J. J. ;. Dapprich, S. ;. Daniels, A. D. ;. Farkas, Ö. ;. Foresman, J. B. ;. Ortiz, J. V. ;. Cioslowski, J. ;. Fox, D. J. *Gaussian 09*; Wallington CT, 2009.

(36) Frisch, M. J.; Trucks, G. W.; Schlegel, H. B.; Scuseria, G. E.; Robb, M. A.; Cheeseman, J. R.; Scalmani, G.; Barone, V.; Petersson, G. A.; Nakatsuji, H.; Li, X.; Caricato, M.; Marenich, A. V.; Bloino, J.; Janesko, B. G.; Gomperts, R.; Mennucci, B.; Hratchian, H. P.; Ortiz, J. V.; Izmaylov, A. F.; Sonnenberg, J. L.; Williams; Ding, F.; Lipparini, F.; Egidi, F.; Goings, J.; Peng, B.; Petrone, A.; Henderson, T.; Ranasinghe, D.; Zakrzewski, V. G.; Gao, J.; Rega, N.; Zheng, G.; Liang, W.; Hada, M.; Ehara, M.; Toyota, K.; Fukuda, R.; Hasegawa, J.; Ishida, M.; Nakajima, T.; Honda, Y.; Kitao, O.; Nakai, H.; Vreven, T.; Throssell, K.; Montgomery Jr., J. A.; Peralta, J. E.; Ogliaro, F.; Bearpark, M. J.; Heyd, J. J.; Brothers, E. N.; Kudin, K. N.; Staroverov, V. N.; Keith, T. A.; Kobayashi, R.; Normand, J.; Raghavachari, K.; Rendell, A. P.; Burant, J. C.; Iyengar, S. S.; Tomasi, J.; Cossi, M.; Millam, J. M.; Klene, M.; Adamo, C.; Cammi, R.; Ochterski, J. W.; Martin, R. L.; Morokuma, K.; Farkas, O.; Foresman, J. B.; Fox, D. J. *Gaussian 16 Rev. A.03*; Wallingford, CT, 2016.

(37) Grimme, S.; Antony, J.; Ehrlich, S.; Krieg, H. A Consistent and Accurate Ab Initio Parametrization of Density Functional Dispersion Correction (DFT-D) for the 94 Elements H-Pu. *J Chem Phys* **2010**, *132* (15), 154104. https://doi.org/10.1063/1.3382344.

(38) Grimme, S.; Ehrlich, S.; Goerigk, L. Effect of the Damping Function in Dispersion Corrected Density Functional Theory. *J. Comput. Chem.* **2011**, *32* (7), 1456–1465. https://doi.org/10.1002/jcc.21759.

(39) Shaik, S.; Kumar, D.; de Visser, S. P.; Altun, A.; Thiel, W. Theoretical Perspective on the Structure and Mechanism of Cytochrome P450 Enzymes. *Chem. Rev.* **2005**, *105* (6), 2279–2328. https://doi.org/10.1021/cr030722j.

(40) Altun, A.; Kumar, D.; Neese, F.; Thiel, W. Multireference Ab Initio Quantum Mechanics/Molecular Mechanics Study on Intermediates in the Catalytic Cycle of Cytochrome P450cam. *J. Phys. Chem. A* **2008**, *112* (50), 12904–12910. https://doi.org/10.1021/jp802092w.

(41) Radoń, M. Spin-State Energetics of Heme-Related Models from DFT and Coupled Cluster Calculations. *J. Chem. Theory Comput.* **2014**, *10* (6), 2306–2321. https://doi.org/10.1021/ct500103h.

(42) Ribeiro, R. F.; Marenich, A. V.; Cramer, C. J.; Truhlar, D. G. Use of Solution-Phase Vibrational Frequencies in Continuum Models for the Free Energy of Solvation. *J. Phys. Chem. B* **2011**, *115* (49), 14556–14562. https://doi.org/10.1021/jp205508z.

(43) Rydberg, P.; Sigfridsson, E.; Ryde, U. On the Role of the Axial Ligand in Heme Proteins: A Theoretical Study. *J Biol Inorg Chem* **2004**, *9* (2), 203–223. https://doi.org/10.1007/s00775-003-0515-y.

(44) Lai, W.; Chen, H.; Shaik, S. What Kinds of Ferryl Species Exist for Compound II of Chloroperoxidase? A Dialog of Theory with Experiment. *J. Phys. Chem. B* **2009**, *113* (22), 7912–7917. https://doi.org/10.1021/jp902288q.

(45) Derat, E.; Shaik, S. Two-State Reactivity, Electromerism, Tautomerism, and "Surprise" Isomers in the Formation of Compound II of the Enzyme Horseradish Peroxidase from the Principal Species, Compound I. *J. Am. Chem. Soc.* **2006**, *128* (25), 8185–8198. https://doi.org/10.1021/ja0600734.
(46) Zederbauer, M.; Jantschko, W.; Neugschwandtner, K.; Jakopitsch, C.; Moguilevsky, N.; Obinger, C.; Furtmüller, P. G. Role of the Covalent Glutamic Acid 242−Heme Linkage in the Formation and Reactivity of Redox Intermediates of Human Myeloperoxidase. *Biochemistry* **2005**, *44* (17), 6482–6491. https://doi.org/10.1021/bi0501737.
(47) Derat, E.; Cohen, S.; Shaik, S.; Altun, A.; Thiel, W. Principal Active Species of Horseradish Peroxidase, Compound I: A Hybrid Quantum Mechanical/Molecular Mechanical Study. *J. Am. Chem. Soc.* **2005**, *127* (39), 13611–13621. https://doi.org/10.1021/ja0534046.
(48) Lai, W.; Chen, H.; Cho, K. B.; Shaik, S. Effects of Substrate, Protein Environment, and Proximal Ligand Mutation on Compound I and Compound 0 of Chloroperoxidase. *J Phys Chem A* **2009**, *113* (43), 11763–11771. https://doi.org/10.1021/jp902898s.
(49) Rydberg, P.; Ryde, U.; Olsen, L. Sulfoxide, Sulfur, and Nitrogen Oxidation and Dealkylation by Cytochrome P450. *J. Chem. Theory Comput.* **2008**, *4* (8), 1369–1377. https://doi.org/10.1021/ct800101v.
(50) Lonsdale, R.; Fort, R. M.; Rydberg, P.; Harvey, J. N.; Mulholland, A. J. Quantum Mechanics/Molecular Mechanics Modeling of Drug Metabolism: Mexiletine N-Hydroxylation by Cytochrome P450 1A2. *Chem. Res. Toxicol.* **2016**, *29* (6), 963–971. https://doi.org/10.1021/acs.chemrestox.5b00514.
(51) Ji, L.; Zhang, J.; Liu, W.; de Visser, S. P. Metabolism of Halogenated Alkanes by Cytochrome P450 Enzymes. Aerobic Oxidation versus Anaerobic Reduction. *Chemistry – An Asian Journal* **2014**, *9* (4), 1175–1182. https://doi.org/10.1002/asia.201301608.
(52) Sono, M.; Dawson, J. H.; Hager, L. P. Ligand and Halide Binding Properties of Chloroperoxidase: Peroxidase-Type Active Site Heme Environment with Cytochrome P-450 Type Endogenous Axial Ligand and Spectroscopic Properties. *Biochemistry* **1986**, *25* (2), 347–356. https://doi.org/10.1021/bi00350a011.
(53) Ikeda-Saito, M. A Study of Ligand Binding to Spleen Myeloperoxidase. *Biochemistry* **1987**, *26* (14), 4344–4349. https://doi.org/10.1021/bi00388a024.
(54) Furtmüller, P. G.; Arnhold, J.; Jantschko, W.; Pichler, H.; Obinger, C. Redox Properties of the Couples Compound I/Compound II and Compound II/Native Enzyme of Human Myeloperoxidase. *Biochemical and Biophysical Research Communications* **2003**, *301* (2), 551–557. https://doi.org/10.1016/S0006-291X(02)03075-9.
(55) Yosca, T. H.; Behan, R. K.; Krest, C. M.; Onderko, E. L.; Langston, M. C.; Green, M. T. Setting an Upper Limit on the Myoglobin Iron(IV)Hydroxide PKa: Insight into Axial Ligand Tuning in Heme Protein Catalysis. *J. Am. Chem. Soc.* **2014**, *136* (25), 9124–9131. https://doi.org/10.1021/ja503588n.
(56) Behan, R. K.; Green, M. T. On the Status of Ferryl Protonation. *Journal of Inorganic Biochemistry* **2006**, *100* (4), 448–459. https://doi.org/10.1016/j.jinorgbio.2005.12.019.
(57) Green, M. T. CH Bond Activation in Heme Proteins: The Role of Thiolate Ligation in Cytochrome P450. *Current Opinion in Chemical Biology* **2009**, *13* (1), 84–88. https://doi.org/10.1016/j.cbpa.2009.02.028.
(58) Smulevich, G.; Hu, S.; Rodgers, K. R.; Goodin, D. B.; Smith, K. M.; Spiro, T. G. Heme-Protein Interactions in Cytochrome c Peroxidase Revealed by Site-Directed Mutagenesis and Resonance Raman Spectra of Isotopically Labeled Hemes. *Biospectroscopy* **1996**, *2* (6), 365–376. https://doi.org/10.1002/(SICI)1520-6343(1996)2:6<365::AID-BSPY3>3.0.CO;2-2.

(59) Smulevich, G.; Feis, A.; Howes, B. D. Fifteen Years of Raman Spectroscopy of Engineered Heme Containing Peroxidases: What Have We Learned? *Acc. Chem. Res.* **2005**, *38* (5), 433–440. https://doi.org/10.1021/ar020112q.
(60) Bathelt, C. M.; Mulholland, A. J.; Harvey, J. N. QM/MM Studies of the Electronic Structure of the Compound I Intermediate in Cytochrome c Peroxidase and Ascorbate Peroxidase. *Dalton Trans.* **2005**, No. 21, 3470. https://doi.org/10.1039/b505407a.
(61) Harvey, J. N.; Bathelt, C. M.; Mulholland, A. J. QM/MM Modeling of Compound I Active Species in Cytochrome P450, Cytochrome C Peroxidase, and Ascorbate Peroxidase. *J. Comput. Chem.* **2006**, *27* (12), 1352–1362. https://doi.org/10.1002/jcc.20446.
(62) Kwon, H.; Basran, J.; Devos, J. M.; Suardíaz, R.; van der Kamp, M. W.; Mulholland, A. J.; Schrader, T. E.; Ostermann, A.; Blakeley, M. P.; Moody, P. C. E.; Raven, E. L. Visualizing the Protons in a Metalloenzyme Electron Proton Transfer Pathway. *Proc Natl Acad Sci USA* **2020**, *117* (12), 6484–6490. https://doi.org/10.1073/pnas.1918936117.
(63) Lee, H. C.; Booth, K. S.; Caughey, W. S.; Ikeda-Saito, M. Interaction of Halides with the Cyanide Complex of Myeloperoxidase: A Model for Substrate Binding to Compound I. *Biochimica et Biophysica Acta (BBA) - Protein Structure and Molecular Enzymology* **1991**, *1076* (2), 317–320. https://doi.org/10.1016/0167-4838(91)90285-8.